

Electronic properties and bonding in ZrH_x thin films investigated by valence-band x-ray photoelectron spectroscopy

Martin Magnuson,^{*} Susann Schmidt, Lars Hultman, and Hans Högborg

Thin Film Physics Division, Department of Physics, Chemistry and Biology (IFM), Linköping University, SE-58183 Linköping, Sweden

(Received 24 May 2017; revised manuscript received 20 September 2017; published 1 November 2017)

The electronic structure and chemical bonding in reactively magnetron sputtered ZrH_x ($x = 0.15, 0.30, 1.16$) thin films with oxygen content as low as 0.2 at.% are investigated by $4d$ valence band, shallow $4p$ core-level, and $3d$ core-level x-ray photoelectron spectroscopy. With increasing hydrogen content, we observe significant reduction of the $4d$ valence states close to the Fermi level as a result of redistribution of intensity toward the H $1s$ -Zr $4d$ hybridization region at ~ 6 eV below the Fermi level. For low hydrogen content ($x = 0.15, 0.30$), the films consist of a superposition of hexagonal closest-packed metal (α phase) and understoichiometric δ - ZrH_x (CaF_2 -type structure) phases, while for $x = 1.16$, the films form single-phase ZrH_x that largely resembles that of stoichiometric δ - ZrH_2 phase. We show that the cubic δ - ZrH_x phase is metastable as thin film up to $x = 1.16$, while for higher H contents the structure is predicted to be tetragonally distorted. For the investigated $\text{ZrH}_{1.16}$ film, we find chemical shifts of 0.68 and 0.51 eV toward higher binding energies for the Zr $4p_{3/2}$ and $3d_{5/2}$ peak positions, respectively. Compared to the Zr metal binding energies of 27.26 and 178.87 eV, this signifies a charge transfer from Zr to H atoms. The change in the electronic structure, spectral line shapes, and chemical shifts as a function of hydrogen content is discussed in relation to the charge transfer from Zr to H that affects the conductivity by charge redistribution in the valence band.

DOI: [10.1103/PhysRevB.96.195103](https://doi.org/10.1103/PhysRevB.96.195103)

I. INTRODUCTION

Zirconium hydrides are important in many applications in the nuclear industry [1], in getter vacuum pumps, as hydrogen storage, in powder metallurgy, and as zircaloy [2]. The hardness, ductility, and tensile strength of ZrH_x alloys can be controlled by varying the hydrogen content [3]. Increasing the H content results in substoichiometric δ - ZrH_x phase (CaF_2 -type structure, $x = \sim 1.6$ – 2 [4] as shown in Fig. 1) and a body-centered tetragonal ϵ phase ($x = 1.75$ – 2) with a ThH_2 -type structure [5] has also been observed [4]. The δ - ZrH_x structure originates from inserting H atoms to occupy all or parts of the tetrahedral interstitials in the CaF_2 structure. Hydrogen acts as a hardening element that prevents dislocation movements and the hydride material becomes a ceramic that is harder, but less ductile than Zr metal [6].

Traditionally, bulk Zr hydrides are synthesized by annealing Zr metal in hydrogen gas for a time period of days to a few weeks at high temperatures between 400 and 900 °C for a homogeneous diffusion process at different H contents [7]. However, defects in the bulk of the Zr metal result in variations in the diffusion rate for hydrogen that cause ZrH_x alloys with composition gradients and less well-defined polycrystalline structure including grain boundaries. At room temperature in air, ZrH_x quickly forms a nanometer-thin surface oxide layer that prevents further oxidation into the bulk. With increased annealing temperature, oxygen proceeds deeper into the bulk of the material, in particular along grain boundaries [8], and a few percent of oxygen cannot be avoided with the annealing-diffusion hydration synthesis method. Consequently, the above conditions hinder adequate bonding determination in hydrides by spectroscopy.

Previous experiments on bulk ZrH_x using ultraviolet photoelectron spectroscopy showed significant changes in the

electronic structure for high hydrogen contents ($x = 1.63$ – 1.94) both at the states near the Fermi level (E_F) and in deeper-lying states around -7 eV [9]. These changes were associated with a phase transition from a cubic (fcc) structure to a face-centered tetragonal (fct) structure as a result of spontaneous symmetry breaking that removes the degeneracy by a distortion known as the Jahn-Teller effect [10] that lowers the total energy of the $4d^25s^2$ electron configuration in the Zr valence band.

For high hydrogen contents ($x = 1.63$ – 1.9), core-level x-ray photoelectron spectroscopy (XPS) studies of bulk ZrH_x materials indicated a significant shift of the Zr $4p$ and $3d$ core levels by 1.0 and 0.7 eV [7], respectively. For $x = 1.52$ – 1.68 , valence-band XPS also showed an interstitial Zr–H bonding peak around 6.4 eV below E_F [11]. Although these studies indicate significant changes in the Zr–H bond for different hydrogen contents, the spectra are affected by superimposed O $2p$ states that occur in the same energy region (5–8 eV) as the Zr–H bonding structures [12].

For the ZrH_x thin films in this work, we apply XPS at the Zr $3d$, $4p$ core levels and the $4d$ valence band to investigate the electronic structures to determine the chemical bonding and conductivity properties as a function of relatively low hydrogen content ($x = 0.15, 0.30$, and 1.16) and compare the result to bulk α -Zr as reference. These hydride compositions were chosen to obtain a spread in the type and amount of Zr–H bonds. Deposited δ - ZrH_x films with CaF_2 -type structure are found to be stable outside the homogeneity region determined for bulk δ - ZrH_2 with compositions ranging from about $\text{ZrH}_{1.5}$ to stoichiometric [13]. To control the structure and hence the electronic properties of the materials and to overcome the problems with oxidation, we deposited homogeneous thin films of ZrH_x using reactive direct current magnetron sputtering (rDCMS). The thin films were grown without external heating and contamination of oxygen, and other contaminants were very low. Thin films are particularly

^{*}Corresponding author: Martin.Magnuson@liu.se

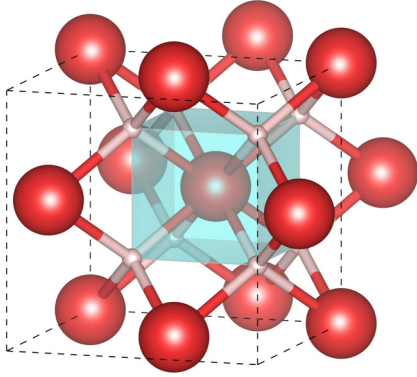


FIG. 1. Unit cell of stoichiometric δ -ZrH₂ (space group 225) with Zr-atoms (red spheres) in $(0,0,0)$, $(\frac{1}{2},\frac{1}{2},0)$, $(\frac{1}{2},0,\frac{1}{2})$, and $(0,\frac{1}{2},\frac{1}{2})$ and with H (white spheres) in all tetrahedral sites $(\frac{3}{4},\frac{1}{4},\frac{1}{4})$, $(\frac{1}{4},\frac{3}{4},\frac{1}{4})$, $(\frac{1}{4},\frac{1}{4},\frac{3}{4})$, $(\frac{3}{4},\frac{3}{4},\frac{3}{4})$, $(\frac{1}{4},\frac{1}{4},\frac{1}{4})$, $(\frac{3}{4},\frac{3}{4},\frac{1}{4})$, $(\frac{1}{4},\frac{3}{4},\frac{3}{4})$, and $(\frac{3}{4},\frac{1}{4},\frac{1}{4})$.

favorable for correct characterization of the material's fundamental bonding properties and to identify different phases in understoichiometric transition-metal hydrides.

II. EXPERIMENTAL

A. Thin-film deposition and XRD characterization

The Zr-H films studied were deposited on Si(100) substrates by rDCMS. ZrH_x films with $x = 0.15, 0.30$, and 1.16 were deposited in an industrial high-vacuum coating system (CemeCon AG, Würselen, Germany). Here, a zirconium target was sputtered in Ar (99.9997%)/H₂ (99.9996% mixtures using a fixed Ar partial pressure of 0.42 Pa with 5, 10, and 20% H₂. The substrate bias was set to -80 V and no external substrate heating was applied. The films were deposited for 120 s, resulting in films with thicknesses ranging between ~ 800 and ~ 840 nm. More detailed information on the deposition conditions is presented in Ref. [14]. The investigated α -Zr reference sample was a commercial zirconium target with a purity of 99.9% (Kurt J. Lesker Company, Clairton, PA, USA).

B. XPS measurements

Valence-band (VB) and XPS measurements of the Zr $3d$, $4p$, $4d$ valence band and O $1s$ core-level regions were performed in a surface analysis system (AXIS UltraDLD, Kratos, Manchester, UK) using monochromatic Al- K_{α} (1486.6 eV) radiation with an incidence angle of 54° and a spot size of $300 \times 800 \mu\text{m}$. The electron energy analyzer detected photoelectrons perpendicular to the sample surface with an acceptance angle of $\pm 15^{\circ}$. The spectra were recorded with a step size of 0.1 eV and a pass energy of 10 eV, which provided an overall energy resolution better than 0.5 eV. The binding-energy scale of all XPS spectra was referenced to the E_F , which was set to a binding energy of 0 eV [15]. The ZrH_x thin films in this work were examined before and after Ar⁺ sputtering for 600 s using an Ar⁺ incident angle of 20° at 4 keV rastered over an area of $2 \times 2 \text{ mm}^2$.

C. Structural model and density-functional theory calculations

The geometry relaxation was performed using the Perdew-Burke-Ernzerhof (PBE) functional [16] including the

Grimme-van der Waals density-functional theory (DFT)-D2 scheme [17]. The first-principle calculations were carried out using DFT implemented in the Vienna *ab initio* simulation package (VASP) [18] with an exchange-potential functional using the general gradient approximation (GGA). A hydrogen-potential suited for short bonds (hydrogen projected augmented wave (PAW) potential H_h) with an energy cutoff of 1050 eV was used. For the self-consistent calculations, the PAW [19] method was used with the PBE and the Heyd-Scuseria-Ernzerhof functionals of the GGA. The HSE06 functional [20] is a hybrid functional including a linear combination of short and long-range PBE exchange terms and a short-range Hartree-Fock term that improves the formation energies and band gaps and peak positions. The screening parameter of HSE06 was 0.2 \AA^{-1} with a plane-wave cutoff energy of 700 eV. A $29 \times 29 \times 29$ k grid was used for the standard PBE functional for the structure relaxation and an $11 \times 11 \times 1$ k grid was used for the HSE06 functional as the computational cost is significantly higher for the HSE06 in comparison to the PBE functional. Using the HSE06 exchange-correlation functional, the energy positions of the bands are shifted by ~ 1.8 eV toward higher energy relative to the E_F , and are thus much more realistic, in comparison to the corresponding energy positions, using the PBE functional. The charge-transfer calculations between the different elements were made using standard Bader analysis [21].

III. RESULTS AND DISCUSSION

Figure 2 shows Zr $3d$ core-level XPS spectra of the ZrH_x thin films in comparison to α -Zr metal. As observed, there is a significant chemical shift toward higher binding energies for the film grown with hydrogen in the plasma compared to the pure metal film, which is a consequence of the higher electronegativity of H ($\chi = 2.2$) in comparison to Zr ($\chi = 1.33$) [22]. For $x = 1.16$, the Zr $3d_{5/2}$ peak position was determined to 179.38 eV. This is in good agreement with the Zr $3d_{5/2}$ binding energy of 179.375 reported for bulk δ -ZrH_{1.74} [23] as well as 179 eV determined for bulk ZrH_{1.9} material [24] and close to the 180-eV binding energy determined for bulk ZrH_{1.64} [25] and ZrH_{1.9} [7]. Furthermore, the position of the $3d_{5/2}$ peak is more or less identical to the binding energy determined for the reactively sputtered ZrH_{1.64} film in Ref. [14] with 179.44 eV. Note the small energy shift toward lower binding energy for the less hydrogen-rich film with $x = 1.16$ (179.38 eV) that is consistent with a smaller charge transfer from Zr to H in this film in comparison to the $x = 1.64$ film (179.44 eV). In addition, for the ZrH_{1.16} film, there is a high-energy shift of +0.51 eV while between $x = 0.15$ and 0.30 , the Zr $3d$ core-level high-energy shift is much smaller (+0.06 eV) and is an indication of smaller average charge transfer from Zr toward H in these samples.

The metallic reference sample has the Zr $3d_{5/2}$ and Zr $3d_{3/2}$ peak positions at 178.87 and 181.28 eV (2.41-eV peak splitting) in good agreement with literature values [26]. The Zr $3d_{5/2}$ - $3d_{3/2}$ spin-orbit splitting is the same in the films. Prior to sputtering, the spectra showed structures of ZrO₂ following air exposure, but at the Zr $3d$ edge after sputtering there are no features connected to oxygen.

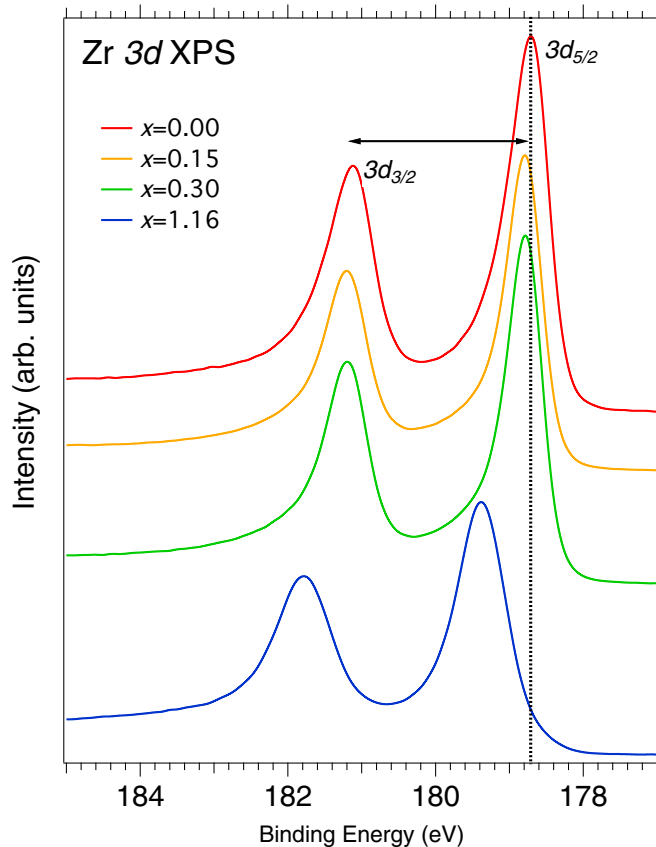


FIG. 2. Zr $3d$ core-level XPS spectra of the ZrH_x thin films in comparison to α -Zr metal. The $3d_{5/2,3/2}$ spin-orbit splitting (2.41 eV) is indicated by the horizontal arrow.

To evaluate the asymmetric tails toward higher binding energies in each spectrum, a Doniac-Sunjic function [27] corresponding to the electron-hole pair excitations created at the Fermi level to screen the core-hole potential was applied. The Doniac-Sunjic profile is essentially a convolution between a Lorentzian with the function $1/E(1-\alpha)$, where E is the binding energy of each peak and α is a parameter known as the *singularity index* that is related to the electron density of states at the Fermi level [28]. The intensities of the tails are related to the amount of metallicity in the system due to the coupling of the core-hole with collective electron oscillations. For α -Zr, the singularity index is large ($\alpha = 0.15$) and the $3d_{5/2}/3d_{3/2}$ branching ratio is higher (1.75) than the statistical value of 1.67 (5/3), signifying high conductivity. For $x = 0.15$ and 0.30, the singularity index and branching ratio remain almost the same as for α -Zr, but for $x = 1.16$, the tail becomes significantly smaller with a singularity index of only $\alpha = 0.04$ with a branching ratio that is smaller (1.61) than the statistical ratio (1.67). This shows that the number of bands crossing the E_F are reduced and thus the expected conductivity.

Figure 3 shows Zr $4p$ shallow core-level XPS spectra of the ZrH_x thin films in comparison to α -Zr metal. As in the case of the Zr $3d$ level, the largest chemical shift of +0.68 eV from 27.26 eV in the metal to 27.94 eV is found for the film with $x = 1.16$, while a smaller shift of 0.1 eV occur for $x = 0.30$ with a similar shift in the composition range $x = 0.15$. The binding energy determined for the Zr $4p_{3/2}$ peak of the

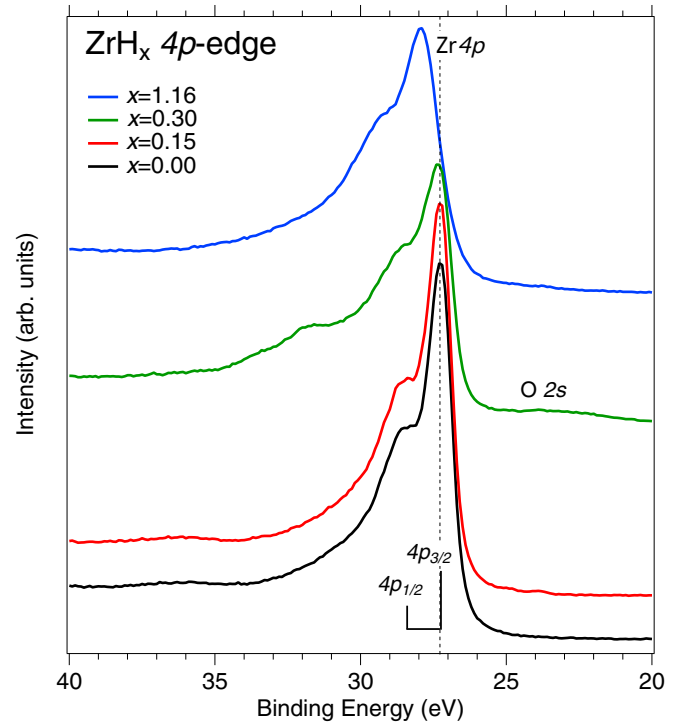


FIG. 3. Zr $4p$ core-level XPS spectra of the ZrH_x thin films in comparison to α -Zr metal. The $4p_{3/2,1/2}$ spin-orbit splitting (1.3 eV) is indicated by the vertical lines, from Ref. [26].

hydride with $x = 1.16$ is slightly lower than the 28.1- and 28.0-eV values reported in Refs. [9] and [12], respectively. For both these studies, the spectra were recorded for oxidized bulk samples, where the interaction of Zr atoms with O causes the Zr $4p$ peak to shift to a higher binding energy. Finally, the $4p_{3/2}$ peak position of the metal reference of 27.26 eV is in agreement with the reported value of 27.1 eV in Ref. [26].

The observed binding energies of the α -Zr spin-orbit split $4p_{3/2,1/2}$ levels are 27.26 and 28.60 eV (1.3 eV splitting). This is consistent with tabulated values of 27.1 and 28.5 eV [26]. At the shallow Zr $4p$ level, we observe both a significant broadening of the spectra and a high-energy shift in the binding energy relative to metallic α -Zr. Only for the film with $x = 0.30$ some oxygen is left even after sputtering. This was also observed by time-of-flight energy elastic recoil detection analysis (ToF-ERDA) showing a slightly higher oxygen content of 0.7% for this film [14] compared to 0.2% for the films with $x = 0.15$ and 1.16.

Figure 4 shows a set of high-resolution VBs XPS spectra of the ZrH_x thin films (0.15, 0.30, and 1.16) in comparison to α -Zr metal. In the region 0–2 eV from the E_F , the spectra are dominated by the Zr $4d$ valence states with a $4d_{5/2-3/2}$ spin-orbit splitting of ~ 1.3 eV, most clearly observed in pure α -Zr ($x = 0$). For $x = 0.15$, the shape of the VB-XPS spectrum is very similar to that of pure α -Zr with a larger broadening and appears to be very little affected by the small hydrogen content. On the contrary, for $x = 1.16$, a major spectral redistribution of intensity changes of the shape of the Zr $4d$ band is further broadened so that the spin-orbit splitting is no longer resolved. The most prominent new feature appears around 6 eV binding energy and is due to the

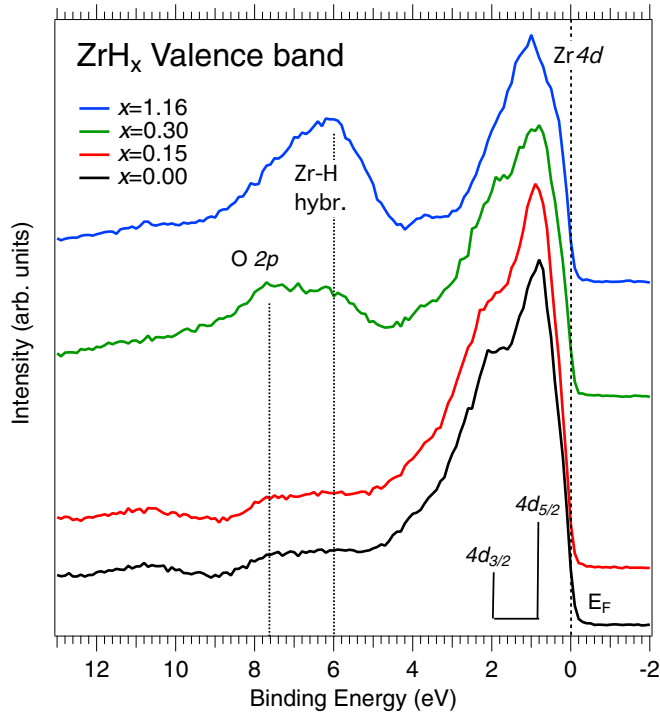


FIG. 4. Valence-band XPS spectra of the ZrH_x thin films in comparison to α -Zr metal.

strong H $1s$ -Zr $4d$ hybridization and bonding. For $x = 0.30$, a significant broadening of the Zr $4d$ valence states at ~ 1 eV is observed. The largest change is in the double-peaked feature between 6 and 7.8 eV. This feature is consistent with previous observations in bulk material [23] with δ -ZrH_{1.52}, δ -ZrH_{1.65}, and δ -ZrH_{1.74}, where the height of the Zr $4d$ peak close to E_F decreases and the Zr-H bonding peak increases with increasing hydrogen content. These observations suggested a donation of Zr $4d$ electrons toward the Zr-H bond, while the Zr-Zr bond weakens. For higher hydrogen content ($x = 1.94$) the states closest to the E_F were enhanced due to a fcc-fct phase transition [9]. However, bulk materials are often hampered by the appearance of superimposed O $2p$ states between 5 and 10 eV, i.e., in the same energy region as the Zr-H bonding peak. As ZrO₂ is known to have prominent peaks of O $2p$ states between 5 and 10 eV and O $2s$ states around 22.5 eV from the E_F [12]. Thus, in bulk materials, the contribution of the Zr-H bond peak cannot be fully distinguished or separated (disentangled) from the O $2p$ states due to oxygen impurities.

Figure 5 shows calculated density of states (DOS) for crystalline δ -ZrH _{x} for $x = 0, 0.5, 1.0, 1.5,$ and 2.0 . As observed, for $x = 0$, the states within 4 eV from the E_F are dominated by Zr $4d$ states while strong Zr $4p$ states occur at 29–30 eV from E_F . This is also the case for increasing x but a prominent peak in the energy region 5–10 eV is mainly due to H $1s$ states that does not exist in pure Zr. At 5–10 eV below E_F , bonding H-H $s-s$ σ , Zr-H $d-s$ σ , and Zr-Zr $d-d$ σ -interactions occur while antibonding H-H $s-s$ σ^* interactions appear above E_F . We find that the H $1s$ character in δ -ZrH _{x} strongly depends on the hydrogen content and increases with x . Notably, a deep DOS minimum at 2–4 eV occurs for $x = 0.5$ when hydrogen is introduced. Closer to the E_F , Zr $4d-e_g$ states dominate at

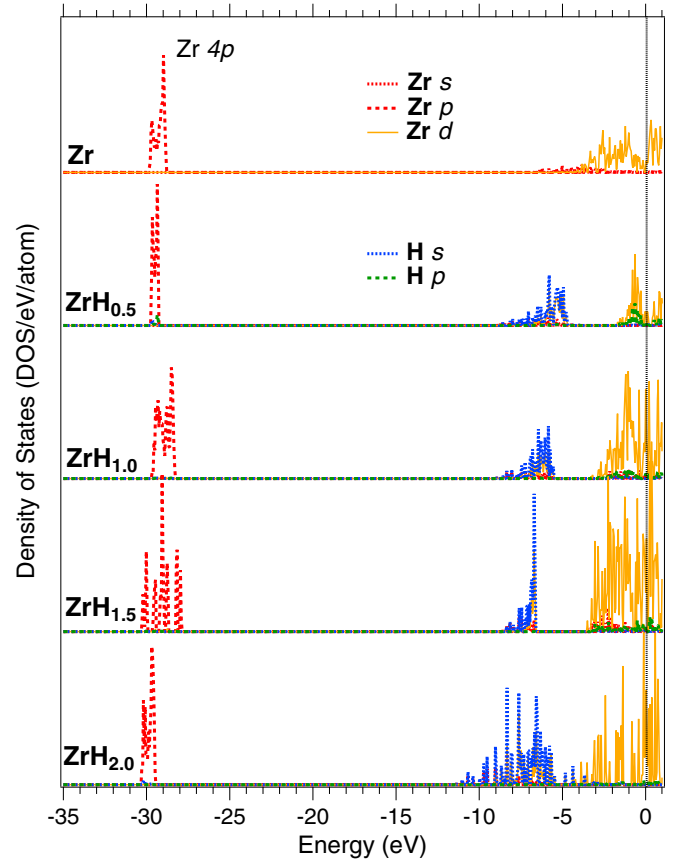


FIG. 5. Calculated DOS for α -Zr and δ -ZrH _{x} , where $x = 0.5, 1.0, 1.5,$ and 2.0 . To enhance the valence bands, the intense Zr $4p$ states at -30 eV were scaled down by a factor of 5.

0–2 eV while H $1s$ states are negligible. For δ -ZrH₂, there is an intense peak at the E_F of Zr $4d-t_{2g}$ character that dominates and causes instability of the crystal structure at 0 K. At finite temperature, phonon interactions and tetragonal (Jahn-Teller) distortion of the structure leads to a splitting of the intense t_{2g} peak at the E_F and a pseudogap develops. This leads to lowering of the total energy of the system and restabilization of the structure. Thus, the t_{2g} states at E_F are reduced at finite temperatures and likely reduce the conductivity and other transport properties. This is consistent with previous DFT studies including the δ - and ϵ phases [29–32] of ZrH _{x} while comparisons to experimental electronic structure studies of the Zr-H bonds of thin films have been lacking. Thus, the order and bonding of the hydrogen atoms in the octahedral sites has not been well understood.

Figure 6 shows the structures (left) and calculated total energies (right) of ZrH _{x} for $x = 0.5, 1.0, 1.5,$ and 2.0 (top to bottom). Here, Jahn-Teller distortion is predicted for high hydrogen content ($x > 1$), where the cubic δ structure becomes unstable and lowers the symmetry. On the contrary, for low hydrogen content, the cubic structure is stable ($x = 0.5$) or metastable ($x = 1.0$). For $x = 2.0$, the minimum of c/a is located at 0.886, for $x = 1.5$ at 0.868, while for $x = 1$ there is a metastable state for $c/a = 1.0$ and a lowest stable state for $c/a = 0.792$. Thus, the cubic δ -ZrH _{x} phase is metastable as thin film up to $x = 1.16$, while for higher H contents the ZrH _{x} structure is predicted to be distorted by the Jahn-Teller effect.

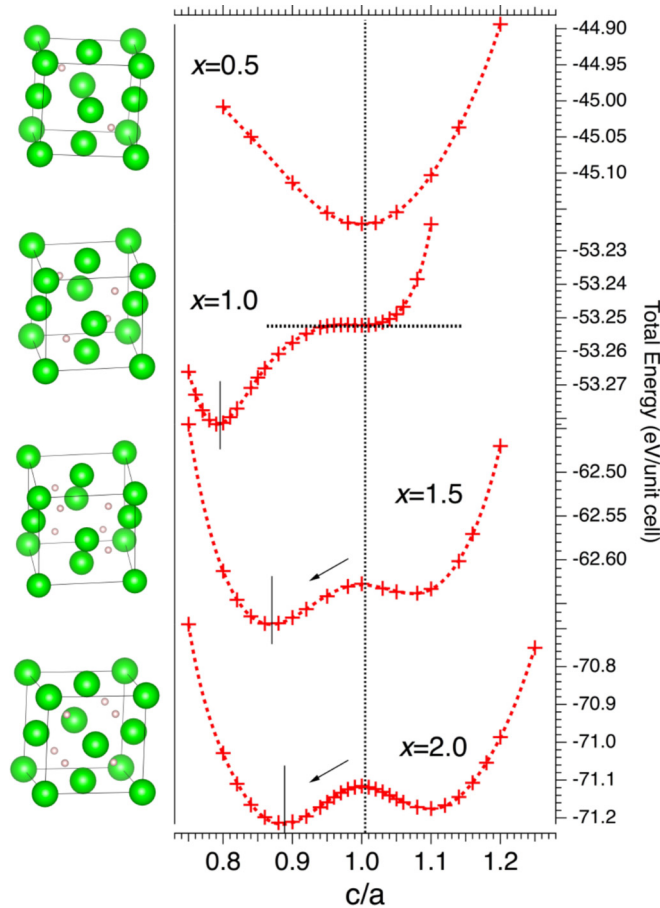


FIG. 6. (Left panel): Model structures. (Right panel): Calculated total energies for ZrH_x, where $x = 0.5, 1.0, 1.5,$ and 2.0 .

To evaluate the charge-transfer dependence on x , we calculated the Bader charges that are listed in Table I together with the lattice parameters for different compositions. Unit cells of δ -ZrH _{x} (Fig. 6, left panels), where the H atoms were replaced by vacancies, were used as model systems for different x . Among the hydrides, the structure and stability properties of ZrH₂ have been of particular interest where the attention has been focused on the δ - ϵ phase transition induced by stress, and the influence of the Jahn-Teller distortion to stabilize the structure [30,33]. As the electronegativity of Zr (1.33) is lower than for H (2.2), the formal oxidation states of H and Zr in ZrH₂ are -1 and $+2$, respectively. Generally, the predicted charge transfer from Zr increases with increasing x and lattice parameter. In comparison to the pure Zr and H

TABLE I. Calculated lattice parameters and charge transfer for ZrH _{x} for different x . Experimental values for α -Zr are given in parenthesis [34].

System	a -lattice parameter	c -lattice parameter	Zr	H
α -Zr	3.2577 (3.2327)	5.1358 (5.1493)	0	–
ZrH _{0.5}	4.6484	4.6607	+0.439 e	–0.878 e
ZrH _{1.0}	4.7457	4.7457	+0.845 e	–0.845 e
ZrH _{1.5}	4.7554	4.75547	+1.175 e	–0.783 e
ZrH _{2.0}	4.7811	4.78117	+1.491 e	–0.745 e

elements, the Bader charge on the Zr atoms in, e.g., ZrH₂, increases significantly by $+1.49e$, i.e., significant charge is withdrawn from the $4d^25s^2$ valence orbitals of Zr. According to the Bader analysis of ZrH₂, the charge is transferred to the lowest unoccupied orbital, of the hydrogen atoms ($1s^1 \rightarrow 1s^{1.75}$), where the Bader charge decreases by $-0.75e$ on each atom. A distortion of the cubic δ -ZrH _{x} structure causes a slight reduction of the charge transfer.

The combined $3d$ and $4p$ core-level and $4d$ valence-band studies show several interesting effects. For the hydride system, we observe a significant reduction of the Zr $4d$ band within ~ 3 eV from the E_F influencing the shallow $4p$ core level by a broadening and an asymmetric redistribution of intensity toward higher binding energy. There is no trace of oxygen on the samples, except for $x = 0.30$, where small signs of O $2p$ and O $2s$ intensity can be distinguished. For the hydrides, a bonding band at 6 eV below the E_F does not occur in pure Zr and is related to strong H $1s$ -Zr $4d$ hybridization. This is also accompanied by a chemical shift with binding energies that are 0.6 eV higher than pure α -Zr indicating significant charge transfer toward H, in particular for $x = 1.16$. In our x-ray absorption near-edge structure study [34], a chemical shift toward higher energies in comparison to Zr metal was found to be due to changes in the oxidation state that depend on the structure and the formation of Zr-H bonding at sufficient hydrogen loading. Previous valence-band XPS experiments have shown a dominant Zr $4d$ peak at 1 eV and another peak around 6.4 eV corresponding to a Zr-H bond [11], consistent with DOS calculations [29–31]. The chemical shift of the Zr edges toward higher bonding energies confirms a significant charge transfer from Zr toward H with increasing hydrogen content. It has been argued that a tetragonal distortion of the cubic δ -ZrH _{x} structure in combination with phonons make the structure stable [30]. However, as shown in Fig. 6, this is only the case for high H content, while at low H content, the cubic structure is stable or metastable and does not distort. Thus, for low H content, the cubic δ structure with tetrahedral Zr sites favorably affects the materials properties in comparison to a tentative octahedral coordination that for hydrogen is inhibited according to the Hagg rules on size, coordination number, and electronegativity.

For ZrH _{x} films deposited by rDCMS, we have previously shown that it is possible to grow films with tailored compositions by altering the concentration of H₂ in the plasma [14]. The properties of the films resemble those of the parent Zr metal where increasing hydrogen content in the films yields higher resistivity seen from the values ranging from ~ 70 to $\sim 120 \mu\Omega \text{ cm}$ in comparison to $42.6 \mu\Omega \text{ cm}$ for α -Zr [35]. The measured hardness values are around 5.5 GPa, which is harder than the ~ 3 GPa determined for bulk α -Zr, using nanoindentation [36].

In studies of bulk ZrH _{x} , there have been problems with oxide, as Zr is known to slowly form stable ZrO₂ on the surface and at the grain boundaries [12]. Previous studies have thus been limited to more or less oxidized polycrystalline bulk materials that contain randomly ordered crystallites with grain boundaries that affect the results of electronic structure characterization. Moreover, investigations of the electronic structures of understoichiometric transition-metal hydrides have been scarce. Thin films synthesized by reactive

magnetron sputtering offer an alternative route to grow metal hydrides such as ZrH_x with well-defined properties and at a fraction of time (deposition time of about 2 min for an 800-nm film) compared to traditional hydration/percolation processes that normally takes 1–2 days or weeks depending on the H content [7]. A further advantage of the films is the low level of contaminants, in particular, the oxygen content that is of the range of 0.2–0.7% as determined by ToF-ERDA [14]. Although 3d core-level shifts in ZrH_x [14] have previously been observed, indicating charge-transfer from Zr to H, a deeper analysis including branching ratio and singularity index is necessary for the understanding how the electronic properties influence the conductivity. For low H content ($x = 0.15$ and 0.30), the films contain a mixture of metallic α -Zr and δ - ZrH_x phases and the metallicity remains. For higher H content ($x = 1.16$), a homogeneous oriented, textured, and understoichiometric δ - ZrH_x phase is formed with a lower singularity index and smaller branching ratio that overall indicate more ceramic properties than for the lower H contents. Producing highly stoichiometric and phase pure materials is thus important for optimizing electrical and hardness properties in a vast number of applications.

IV. CONCLUSIONS

Early transition-metal hydrides are a new class of thin-film materials where the cubic δ - ZrH_x phase is metastable up to $x = 1.16$, while for higher H contents the ZrH_x structure is predicted to be distorted by the Jahn-Teller effect both in thin films and bulk synthesized materials. By combining valence-band and shallow core-level x-ray photoelectron spectroscopy with electronic structure calculations, we have investigated the electronic structure and chemical bonding of ZrH_x thin films

with $x = 0.15, 0.30$, and 1.16 in comparison to α -Zr metal. For the understoichiometric δ - $ZrH_{1.16}$ film, there are significant chemical shifts of 0.68 and 0.51 eV for the $4p_{3/2}$ and $3d_{5/2}$ peak positions toward higher energies compared to the metal values of 27.26 and 178.87 eV. We find that even though there is a significant charge transfer from the Zr 4d states toward the H 1s states in δ - $ZrH_{1.16}$, there are still states crossing the Fermi level that signify metallicity. This is due to the fact that there is a significant asymmetric redistribution of spectral intensity from the shallow Zr 4p core level toward the Zr 4d valence band that accompanies the charge-transfer. There are important changes at the Fermi level with a splitting of the 4d band into a pseudogap where the Fermi level is located in a local minimum that stabilize the structure and minimize the total energy of the system. For the hydrides, a bonding band around 6 eV below the Fermi level does not occur in pure Zr and is related to strong H s–Zr 4d hybridization. This is also accompanied by a chemical shift with binding energies that are 0.68 eV higher than pure α -Zr, indicating significant charge transfer toward H, in particular for $x = 1.16$.

ACKNOWLEDGMENTS

The research leading to these results has received funding from the Swedish Government Strategic Research Area in Materials Science on Functional Materials at Linköping University (Faculty Grant SFO-Mat-LiU No. 2009-00971). M.M. acknowledges financial support from the Swedish Energy Research (Grant No. 43606-1), the Swedish Foundation for Strategic Research (SSF) (Grant No. RMA11-0029) through the synergy grant FUNCASE, and the Carl Trygger Foundation (Grants No. CTS16:303 and No. CTS14:310). Dr. Grzegorz Greczynski is acknowledged for assistance with the measurements of the Zr 3d core-level XPS spectra.

-
- [1] G. D. Moan and P. Rudling, in *Zirconium in the Nuclear Industry: Thirteenth International Symposium* (ASTM International, West Conshohocken, PA, 2002).
 - [2] M. P. Puls, *The Effect of Hydrogen and Hydrides on the Integrity of Zirconium Alloy Components* (Springer, London, 2012).
 - [3] M. V. C. Sastri, *Metal Hydrides: Fundamentals and Applications* (Springer-Verlag, Berlin, 1998).
 - [4] L. Holliger, A. Legris, and R. Besson, Hexagonal-based ordered phases in H-Zr, *Phys. Rev. B* **80**, 094111 (2009).
 - [5] JCPDS-International Centre for Diffraction Data. Zirconium Hydride (ZrH_2) Ref. ID 00-017-0314, <http://www.icdd.com/>.
 - [6] W. M. Mueller and J. P. Blackledge, *Metal Hydrides* (Academic, New York, 1968).
 - [7] T. Riesterer, Electronic structure and bonding in metal hydrides, studied with photoelectron spectroscopy, *Z. Phys. B* **66**, 441 (1987).
 - [8] R. C. Bowman, Jr., B. D. Craft, J. S. Cantrell, and E. L. Venturini, Effects of thermal treatments on the lattice properties and electronic structure of ZrH_x , *Phys. Rev. B* **31**, 5604 (1985).
 - [9] J. H. Weaver, D. J. Peterman, D. T. Peterson and A. Franciosi, Electronic structure of metal hydrides. IV. TiH_x , ZrH_x , HfH_x , and the fcc-fct lattice distortion, *Phys. Rev. B* **23**, 1692 (1981).
 - [10] H. A. Jahn and E. Teller, Stability of polyatomic molecules in degenerate electronic states. I. Orbital degeneracy, *Proc. R. Soc. London A* **161**, 220 (1937).
 - [11] M. Uno, K. Yamada, T. Maruyama, H. Muta, and S. Yamanaka, Thermophysical properties of zirconium hydride and deuteride, *J. Alloys Compd.* **366**, 101 (2004).
 - [12] B. W. Veal, D. J. Lam, and D. G. Westlake, X-ray photoemission spectroscopy study of zirconium hydride, *Phys. Rev. B* **19**, 2856 (1979).
 - [13] T. B. Massalski, J. L. Murray, L. H. Bennett, and H. Baker, *Binary Alloy Phase Diagrams* (American Society for Metals, Metals Park, OH, 1986).
 - [14] H. Högborg, L. Tengdelius, M. Samuelsson, F. Eriksson, E. Broitman, J. Lu, J. Jensen, and L. Hultman, Reactive sputtering of δ - ZrH_2 thin films by high power impulse magnetron sputtering and direct current magnetron sputtering, *J. Vac. Sci. Technol. A* **32**, 041510 (2014).
 - [15] S. Hüfner, *Photoelectron Spectroscopy* (Springer-Verlag, Berlin, 1996).
 - [16] J. P. Perdew, K. Burke, and M. Ernzerhof, Generalized Gradient Approximation Made Simple, *Phys. Rev. Lett.* **77**, 3865 (1996).

- [17] S. Grimme, Semiempirical GGA-type density functional constructed with a long-range dispersion correction, *J. Comput. Chem.* **27**, 1787 (2006).
- [18] G. Kresse and J. Furthmüller, Efficient iterative schemes for *ab initio* total-energy calculations using a plane-wave basis set, *Phys. Rev. B* **54**, 11169 (1996).
- [19] P. E. Blöchl, Projector augmented-wave method, *Phys. Rev. B* **50**, 17953 (1994).
- [20] J. Heyd, G. E. Scuseria, and M. Ernzerhof, Hybrid functionals based on a screened Coulomb potential, *J. Chem. Phys.* **118**, 8207 (2003).
- [21] M. Yu and D. R. Trinkle, Accurate and efficient algorithm for Bader charge integration, *J. Chem. Phys.* **134**, 064111 (2011).
- [22] W. W. Porterfield, *Inorganic Chemistry: A Unified Approach*, 2nd ed. (Academic, New York, 1993).
- [23] S. Yamanaka, K. Yamada, K. Kurosaki, M. Uno, K. Takeda, H. Anada, T. Matsuda, and S. Kabayashi, Characteristics of zirconium hydride and deuteride, *J. Alloys Compd.* **99**, 330 (2002).
- [24] J. D. Corbett and H. S. Marek, A photoelectron spectroscopic study of the zirconium monohalide hydrides and zirconium dihydride. Classification of metal hydrides as conventional compounds, *Inorg. Chem.* **22**, 3194 (1983).
- [25] T. A. Sasaki and Y. Baba, Chemical-state studies of Zr and Nb surfaces exposed to hydrogen ions, *Phys. Rev. B* **31**, 791 (1985).
- [26] R. Nyholm and N. Mårtensson, Core level binding energies for the elements Zr-Te ($Z = 40-52$), *J. Phys. C: Solid State Phys.* **13**, L279 (1980).
- [27] S. Doniach and M. Sunjic, Many-electron singularity in X-ray photoemission and X-ray line spectra from metals, *J. Phys. C* **3**, 285 (1970).
- [28] P. Nozières and C. T. De Dominicis, Singularities in the x-ray absorption and emission of metals. III. One-body theory exact solution, *Phys. Rev.* **178**, 1097 (1969).
- [29] P. Zhang, B.-T. Wang, C.-H. He, and P. Zhang, First-principles study of ground state properties of ZrH_2 original, *Comput. Mater. Sci.* **50**, 3297 (2011).
- [30] W. Wolf and P. Herzig, First-principles investigations of transition metal dihydrides, TH_2 : $T = Sc, Ti, V, Y, Zr, Nb$; energetics and chemical bonding, *J. Phys.: Condens. Matter* **12**, 4535 (2000).
- [31] T. Chihi, M. Fatmi, and A. Bouhemadou, Structural, mechanical and electronic properties of transition metal hydrides MH_2 ($M = Ti, Zr, Hf, Sc, Y, La, V$ and Cr), *Solid State Sci.* **14**, 583 (2012).
- [32] M. Gupta and J. P. Burger, Trends in the electron-phonon coupling parameter in some metallic hydrides, *Phys. Rev. B* **24**, 7099 (1981).
- [33] R. Quijano, R. de Coss, and D. J. Singh, Electronic structure and energetics of the tetragonal distortion for TiH_2 , ZrH_2 , and HfH_2 : A first-principles study, *Phys. Rev. B* **80**, 184103 (2009).
- [34] M. Magnuson, F. Eriksson, L. Hultman, and H. Högberg, Bonding structures of ZrH_x thin films by x-ray spectroscopy, *J. Phys. Chem. C* (2017), doi:10.1021/acs.jpcc.7b03223.
- [35] P. W. Bickel and T. G. Berlincourt, Electrical properties of hydrides and deuterides of zirconium, *Phys. Rev. B* **2**, 4807 (1970).
- [36] M. Kuroda, D. Setoyama, M. Uno, and S. Yamanaka, Nanoindentation studies of zirconium hydride, *J. Alloys Compd.* **368**, 211 (2004).